INL/JOU-20-58950-Revision-1

Construction of a Code Verification Matrix for Heat Conduction With Finite Element Code Applications

December 2020

Aysenur Toptan, Nathan W. Porter, Jason D Hales, Benjamin W Spencer, Martin Pilch, Richard L Williamson

Changing the World's Energy Future

INL is a U.S. Department of Energy National Laboratory operated by Battelle Energy Alliance, LLC

INL/JOU-20-58950-Revision-1

Construction of a Code Verification Matrix for Heat Conduction With Finite Element Code Applications

Aysenur Toptan, Nathan W. Porter, Jason D Hales, Benjamin W Spencer, Martin Pilch, Richard L Williamson

December 2020

Idaho National Laboratory
Idaho Falls, Idaho 83415

http://www.inl.gov

Prepared for the
U.S. Department of Energy
Under DOE Idaho Operations Office
Contract DE-AC07-05ID14517

Construction of a Code Verification Matrix for Heat Conduction with Finite Element Code Applications

Aysenur Toptan
Computational Scientist
Computational Mechanics & Materials
Idaho National Laboratory
P.O. Box 1625, Idaho Falls, ID 83415
Email: aysenur.toptan@inl.gov

Nathan W. Porter
Nuclear Engineer
Structural and Thermal Analysis
Sandia National Laboratories
P.O. Box 5800, Albuquerque, NM 87185

Jason D. Hales
Manager
Computational Mechanics & Materials
Idaho National Laboratory
P.O. Box 1625, Idaho Falls, ID 83415

Benjamin W. Spencer
Computational Scientist
Computational Mechanics & Materials
Idaho National Laboratory
P.O. Box 1625, Idaho Falls, ID 83415

Martin Pilch
Consultant
MPilchConsulting
26 Mustang Mesa Trail, Tijeras, NM 87059

Richard L. Williamson
Emeritus Laboratory Fellow
Computational Mechanics & Materials
Idaho National Laboratory
P.O. Box 1625, Idaho Falls, ID 83415

ABSTRACT

When establishing the pedigree of a simulation tool, code verification is used to ensure that the implemented numerical algorithm is a faithful representation of its underlying mathematical model. During this process, numerical results on various meshes are systematically compared to a reference analytic solution. The selection of analytic solutions can be a laborious process, as it is difficult to establish adequate code confidence without performing redundant work. Here, we address this issue by applying a physics-based process that establishes a set of reference problems. In this process, code simulation options are categorized and systematically tested, which ensures that gaps in testing are easily identified and addressed. The resulting problems are primarily intended for code verification analysis but may also be useful for comparison to other simulation codes, troubleshooting activities, or training exercises. The process is used to select fifteen code verification problems relevant for the one-dimensional steady state heat conduction equation. These problems are applicable to a wide variety of simulation tools, but, in this work, a demonstration is performed using the finite element-based nuclear fuel performance code BISON. Convergence to the analytic solution at the theoretical rate is quantified for a selection of the problems, which establishes a baseline pedigree for the code. Not only can this standard set of conduction solutions be used for verification of other codes, but also the physics-based process for selecting problems can be utilized to quantify and expand testing for any simulation tool.

1 Introduction

Over the last century, the evolution of computational modeling and simulation (M&S) methods has revolutionized the scientific process. M&S tools enable a detailed understanding of complex coupled physical phenomena that are often difficult to explore experimentally. However, if these tools are to be used to inform high-consequence decisions, they must be reliable

and predictive. A variety of processes have been developed to address this issue, and they generally have two fundamental steps: verification and validation [1].

1. *Verification*, which includes the components listed below, is used to ensure that the code functions correctly and is reliable.
   (a) *Software quality assurance (SQA)* is a set of software engineering procedures including revision control, issue tracking, peer review, defect analysis, and automated testing. The main goal of these procedures is to eliminate coding mistakes during software development.
   (b) *Code verification* ensures that the implemented numerical algorithm is a faithful representation of the underlying mathematical model, which includes any differential or integral equations along with any associated initial conditions, boundary conditions, and auxiliary relationships.
   (c) *Solution verification* is the assessment of sources of numerical uncertainty, including round-off, statistical variation, iterative tolerances, and truncation error.
2. *Validation* is the process of assessing a code's capability to accurately model physical problems. Comparisons between code results and experiments quantify this capability.

Note that some literature includes SQA as a part of code verification (e.g., [1, 2]). Here, the two activities are distinguished to clearly separate testing of the numerical algorithm from other testing activities. The application of verification and validation procedures is crucial to the development of computational tools that are free of coding mistakes and that accurately represent reality. Without applying these processes, the results from simulation tools can be unreliable and misleading. Details for all of these processes and related topics and can be found in the literature [1, 3, 4], but this work focuses on the code verification of heat conduction codes.

Heat transfer principles are important to various engineering problems: the thermal design and efficiency of turbine blades, the effective removal of heat in electronic chips, material selection and design, power engineering, etc. The aforementioned applications involve three primary heat transfer mechanisms: conduction, convection, and thermal radiation. In this work, we focus on the code verification of M&S tools that solve the heat conduction equation.

$$\rho c_P \frac{\partial T}{\partial t} - \nabla \cdot (k \nabla T) - q''' = 0 \tag{1}$$

Here, ρ, c_P, and k are respectively the density, specific heat, and thermal conductivity of the material of interest. In most real applications, these properties are temperature-dependent. The quantity of interest is temperature T and q''' is a volumetric heat source. In the most general case, the heat source can account for a variety of physical phenomena, e.g. heat produced by nuclear fission, resistive heating, or induction heating.

The heat flux $\boldsymbol{q''}$ within the solution domain is often of interest, and is computed as

$$\boldsymbol{q''} = -k \nabla T. \tag{2}$$

The heat conduction equation can be subject to a variety of boundary conditions, though only three are considered in this work. A `Type 1` boundary condition, or the Dirichlet boundary condition, is applied as

$$T = \hat{T} \quad \text{on } \Gamma_T, \tag{3}$$

where $\hat{T}$ is the prescribed value of temperature, which is applied on the boundaries Γ_T. A `Type 2` boundary condition, or a Neumann boundary condition, can be applied as

$$-k \nabla T = \hat{q}'' \boldsymbol{n} \quad \text{on } \Gamma_q, \tag{4}$$

where the prescribed heat flux $\hat{q}''$ is applied on boundaries Γ_q in the outward normal direction, and $\boldsymbol{n}$ is the outward normal vector. A `Type 3` boundary condition, or a convective boundary condition, is denoted as

$$-k \nabla T = h(T - T_f) \boldsymbol{n} \quad \text{on } \Gamma_q, \tag{5}$$

where the heat flux normal to the boundaries Γ_q is characterized by convective heat transfer to a fluid with some constant temperature T_f and a heat transfer coefficient h.

We propose a standard set of analytic conduction problems for verification of codes that solve the conduction equation on a discrete mesh. This includes fifteen steady state one-dimensional problems that cover many possible combinations of coordinate system, physics, and boundary conditions. Some problems are harvested from the literature, and others are newly proposed here. This set of problems can be a starting point for analysts aiming to benchmark against other codes, debug their code, train new users, or perform code verification. These problems can be incorporated as automated code verification problems, which will ensure that code development does not disrupt existing capabilities.

The code verification process is demonstrated for three of the standardized problems using BISON, which is a nuclear fuel performance code. BISON models the thermo-mechanical behavior of nuclear fuel using the finite element method (FEM) [5, 6, 7]. The code is based on the Multiphysics Object-Oriented Simulation Environment (MOOSE), which is a high-performance, open-source, C++ finite element framework developed at Idaho National Laboratory (INL) [8]. MOOSE provides a generalized framework for the solution of partial differential equations that can be applied to a large variety of problems, allowing scientists and engineers to focus on the models relevant to their particular field and minimize the need to deal with the details of computational science. In addition to the basic solution framework, MOOSE also includes a set of modules that provide implementations of the models required to solve basic physics equations—such as the heat equation solved here—which may be used in multiple applications. BISON is one of the most well-known application codes that uses MOOSE. Recent work has focused on improving, automating, and documenting code verification in BISON using this standard set of problems, which was selected based on a physics-based process [9].

The code verification methodology is outlined in Section 2. Section 3 describes how to construct a verification test matrix for the heat conduction equation. Section 4 covers the standardized set of verification problems with their analytic solutions. The application of these problems for the code verification of BISON is detailed in Section 5. Lastly, Section 6 concludes this paper with a discussion of the results and future work.

2 Code Verification Methodology

When using complex M&S tools, code output is dependent upon many factors: the selected numerical algorithm, temporal and spatial discretization, iterative tolerances, machine precision, etc. Therefore, a formal proof of correctness is not possible because the code output cannot be precisely predicted [4]. In the absence of a formal proof of correctness, code verification can be used to provide a high degree of confidence that a scientific code is correct. This can be achieved through a quantified demonstration that the code converges to a reference solution at the theoretical rate as the computational mesh and time discretization are refined.

The first task in the verification process is to select a reference solution. In this work, the method of exact solutions (MES) [2] is used to perform code verification, which uses an exact analytic solution as a reference. The mathematical problem must be defined and solved, which involves selecting the conservation terms to be tested, setting boundary conditions and/or initial conditions, and then mathematically solving the analytic problem. In cases where a nontrivial analytic solution is difficult to formulate, the method of manufactured solutions (MMS) [1,2,4,10] can be used to choose a reference solution. However, only analytic reference solutions are used here because MMS requires code flexibility that is not available in most simulation tools. For an example of MMS, see the report upon which this work is based [9].

For heat transfer applications (including heat conduction, convection, and radiation), there are many exact solutions available in the literature. Various institutions have created catalogues of these analytical solutions—with all necessary mathematical details and supporting information—for use by engineers and scientists [11, 12, 13]. New analytical solutions are constantly proposed, such as in [14, 15, 16, 17, 18, 19, 20, 21]. In this work, it is noted when a reference solution is taken from existing literature, and the remaining solutions are newly proposed.

Once the reference solution is selected, the theoretical convergence rate of the numerical algorithm is established. The theoretical rate—known as the formal order of accuracy—can be determined through analysis of the linear truncation error (LTE). The formal order of accuracy is derived in Appendix A for the FEM, and similar analysis techniques can be applied for codes using the finite volume method or finite difference method [1, 22, 23, 24]. It is possible to derive the formal order of accuracy even for complex nonlinear discretization methods [23]. The order of accuracy can also be problem-dependent. For example, the order of accuracy is often degraded in the presence of singularities or discontinuities [25, 26]. Hyper-convergent behavior is expected for problems where the choice of discretization is sufficient to exactly fit the analytic solution. For example, a second-order FEM approximates a quadratic reference solution to within the numerical error.

Once the formal order of accuracy is known, a numerical representation of the mathematical model is formulated and solved on at least three meshes. After the numerical solutions are available, global errors between them and the reference solution are calculated using norms. For example, the L_2 or Euclidean norm of the temperature error over the solution domain

Ω is defined as

$$||T|| = \left[\int_{\Omega} (T - \tilde{T})^2 \mathrm{d}\Omega \right]^{1/2}, \tag{6}$$

where the reference solution temperature is T and the numerical approximation of temperature is $\tilde{T}$. Since the local LTE converges at some rate, this global error will converge at the same rate if the mesh size is (1) small enough to eliminate higher order LTE terms and (2) large enough that numerical error is not dominant. Therefore, the error can be related to the characteristic element size h:

$$||T|| = Ch^{\hat{p}}, \tag{7}$$

where C is an arbitrary problem-dependent constant and $\hat{p}$ is the observed order of accuracy. Since this is a power-law function, the slope of the error on a log-log plot is the observed order of accuracy $\hat{p}$. The observed order of accuracy can be estimated using any regression analysis that fits Eqn. 7 to the calculated global errors. The observed order can be estimated using only two mesh refinement levels:

$$\hat{p} = \frac{\log\left(||T||_{rh} / ||T||_h\right)}{\log(r)}, \tag{8}$$

where $||T||_h$ is the temperature norm at some mesh size h and the mesh refinement factor is r.

In this work, many meshes are examined to understand the convergence behavior over a wide range of mesh sizes. For steady state problems, only the spatial mesh is refined; however, the spatial mesh and temporal discretization can be refined simultaneously for transient problems [1, 27].

In practical applications, the convergence behavior is characterized by three regions as shown in Fig. 1 [28]. When the mesh is coarse, higher order terms degrade the order of accuracy (region *I*). The region analyzed in the code verification process is the *asymptotic region* (region *II*), where the higher order terms are small enough that the observed order approximates the formal order. Finally, when the mesh is highly refined, other sources of numerical error begin to be more dominant than the discretization error; therefore, as the mesh is refined further, there is a leveling-off of the error and even a slight increase as the numerical error accumulates (region *III*). Sources of numerical error that can cause this are typically the iterative tolerance for numerical matrix solvers, statistical error in stochastic simulation codes, and/or round-off error due to machine precision. For problems where the choice of discretization is sufficient to exactly fit the analytic solution, hyper-convergent behavior is expected. Even for coarse meshes, the code approximates the analytic solution to within the numerical error; therefore, region *III* exemplifies the convergence behavior.

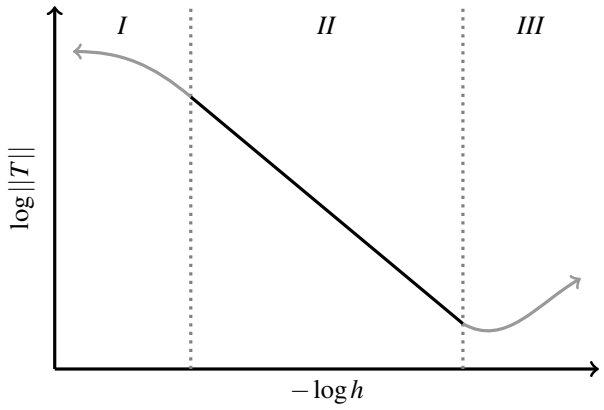

Fig. 1: A pictorial representation of expected convergence behavior. Region *I* represents coarse meshes, region *II* is the asymptotic region, and region *III* is caused by numerical error.

If the convergence behavior is significantly different than Fig. 1, it indicates an error in the reference solution, numerical

model, or post-processing of the simulation results. Debugging and correcting these errors is an integral part of the verification process. The code verification problem is successful if the observed order of accuracy and formal order of accuracy are consistent. The simulation converges to the reference solution at the theoretical rate, which provides confidence in the implemented numerical algorithm. The problem is then used as supporting evidence that the particular combination of physics, discretization, geometry, boundary conditions, and initial conditions is free of coding mistakes.

3 Test Matrix Construction

The selection of reference solutions is an important part of the verification process. An analyst is tasked with providing enough evidence that the numerical algorithm is correct without performing redundant or unnecessary work. This laborious process of selecting test problems can be simplified by providing a standard set of solutions for a particular conservation equation. Once a set of standard problems is established, they can be used to analyze a variety of codes.

One approach for proposing a standard set of problems is to create a large library containing as many analytic solutions as possible. This approach can result in a large set of analytical solutions for engineering applications that (1) is difficult for code analysts to manage and (2) is constantly updated by researchers in the literature. Additionally, incorporating a large library of verification problems into a simulation code can be unnecessarily laborious. Here, a more targeted physics-based approach is introduced to include the minimum number of problems that sufficiently test all considered simulation options. There are six simulation options that must be considered in codes solving the heat conduction equation.

1. Whether the problem is steady state or transient.
2. The simulated coordinate system, which can be Cartesian, cylindrical, or spherical.
3. Dimensionality, which can include one-dimensional, two-dimensional, or three-dimensional solutions.
4. The treatment of solid properties (e.g., thermal conductivity k, density ρ, or specific heat c_P) can deteriorate the observed order of accuracy if not correctly incorporated into the discretized equation. For example, discontinuities in the function or its derivatives can degrade the order of accuracy (e.g., table lookups, piece-wise approximations, or threshold functions).
5. The treatment of external sources q''', which can be implemented incorrectly in numerical algorithms.
6. Chosen boundary conditions, which typically include, but are not limited to, Dirichlet, Neumann, radiative, and convective boundaries. The treatment of initial conditions can also be considered.

Given these six general considerations, a code verification matrix can be created. The matrix is formulated by first incorporating each simulation option into at least one verification problem. Once each option has been tested, the verification matrix is expanded by employing different combinations of these options. This ensures that the coupling between different options does not reveal coding mistakes that are otherwise hidden. Once a matrix is established, it can easily be expanded based on the physics and application of interest. A generalized code verification matrix for the heat conduction equation is shown in Table 1.

This physics-based approach for the construction of code verification matrices allows an analyst to adjust the matrix complexity based upon the physics of interest and the use cases for a particular code. For example, since the thermal conductivity of uranium oxide is temperature-dependent, a verification problem which includes temperature-dependent thermal conductivity is particularly important for modeling nuclear fuel. Therefore, an analyst considering nuclear fuel performance will likely include such a test in their code verification matrix. Additionally, application-specific models can be considered in the construction of the code verification matrix. For example, the nuclear fuel performance code, BISON models the thermal behavior of the gap between two surrounding solids (e.g., the gap between nuclear fuel and cladding, which is filled with an inert gas [9, 29, 30, 31, 32, 33, 34, 35]). Code verification can be performed using an analytic solution that accounts for this model. However, the set of problems proposed in this work excludes application-specific models.

Though a test matrix is a strong tool for summarizing the features tested in a computer code, these tests must also be cataloged in a code's test suite. For this purpose, we employ a naming convention for analytic solutions to the heat conduction equation. This convention is briefly introduced in the next section.

3.1 Numbering System in Heat Conduction

The conventional nomenclature for numbering analytical solutions to the heat conduction equation was originally proposed in [36] and has been gradually extended as additional researchers have used it. The modern version of the nomenclature used in this work (from [37]) is briefly described in Table 2. It is categorized by five characteristics of the problem: (1) boundary conditions, (2) interface conditions, (3) time- and space-variable functions at boundary conditions, (4) space-variable initial conditions, and (5) time-variable source terms.

Though Table 2 covers most characteristics of a heat conduction problem, it does not consider non-constant thermophysical properties. To address this issue, we have taken the notation for the source term (`G`) and boundary conditions (`B`)

Table 1: Generic verification matrix for the heat conduction equation [9].

Problem No.	Transient		Coordinate System			Dimension			Properties and External Sources						Boundary Conditions		
	Transient	Steady State	Cartesian	Cylindrical	Spherical	x_1	x_2	x_3	k	$k(T)$	α_c	$\alpha(T)$	q'''	$q'''(\boldsymbol{x})$	Drichlet	Neumann	Convective

and generalized it to apply to an arbitrary quantity of interest Q. The generalized notation, which is shown in Table 3, allows the quantity of interest to vary with space x, time t, or temperature T. Since it would be inconsistent with curvilinear coordinate systems, x was not introduced to the notation. For example, the notation for the source term is expressed by `G` in Table 2. Therefore, an exponentially space-dependent source term is notated as `G5`, whereas the corresponding exponentially time-dependent source term is `Gt5`. The generalized notation allows for the introduction of additional quantities of interest (e.g., in this work, thermal conductivity is notated as `K`) and allows them to depend on any state variable.

4 A Standard Set of Verification Problems

A standard set of solutions to the conduction equation are presented in this section. Following the process outlined in Section 3, Table 1 is specialized considering only one-dimensional steady state problems. The table incorporates all simulation options into one or more problems. Additionally, most combinations of simulation options are also tested.

The test matrix constructed for the code verification of conduction equations is shown in Table 4. The included simulation options are: coordinate system, constant or temperature-dependent thermal conductivity, constant or spatially-varying internal heat generation, and choice of boundary condition. Each row corresponds to a verification problem that includes the checked simulation options. Five problems are selected with similar settings for each coordinate system, which enables sufficient testing of all coordinate systems in a code. For example, problems I.1, II.1, and III.1 all have constant thermal conductivity and heat generation with Dirichlet boundary conditions. The symmetry between these tests ensures that the coordinate systems are all sufficiently and equally tested.

To place the chosen test problems in context to existing literature, the table also includes the numbering system outlined in Section 3.1. The coordinate systems Cartesian, cylindrical, and spherical are respectively indicated by `X`, `R`, and `RS`. The first two numbers indicate the type of boundary condition applied to the left and right boundary (corresponding to types 1, 2, and 3 in Eqs. 3, 4, and 5). The two numbers after `B` indicate specialization of the corresponding boundary conditions, where `0` indicates a finiteness requirement and `1` indicates a constant. The heat generation (i.e., the source term for the heat conduction equation) is indicated by the number after `G`, where `0` is no heat generation, `1` indicates a constant, and `2` indicates linearly varying heat generation (see Table 3 for the additional numbering based on the functional form). The reference does not yet include notation for the behavior of thermal conductivity, so we use the notation `K`, where `K0` indicates a constant thermal conductivity and `KT1` indicates linear variation with temperature.

Refer to [9] for additional problems not included in this matrix, including multi-dimensional, transient, and MMS problems. However, these groups of problems are not sufficiently developed to create a full verification matrix that tests all simulation options systematically in each coordinate system. Therefore, future work will focus on extending these problems to verification matrices using additional steady-state, quasi steady-state, and transient problems from the literature.

Schematics for each problem are shown in Fig. 2. The detailed description and solution of each problem are provided in Sections 4.1, 4.2, and 4.3 for Cartesian, cylindrical, and spherical coordinates, respectively. For problems from the literature, the original source is cited. Problems without a reference are newly derived in this work (see Appendix B). These problems are included in the physics module tests in the MOOSE repository and analytic solutions for all included problems are included as Python scripts located alongside the corresponding finite element (FE) models.

4.1 Cartesian Coordinates

Problem I.1 (`X11B11G1K1`) An infinite plate with constant thermal conductivity k and internal heat generation q''' is defined in the region $0 \leq x \leq L$. Constant temperatures are imposed on each boundary: $T(x=0) = T_0$ and $T(x=L) = T_L$. This problem is shown schematically in Fig. 2a. Upon reaching thermal equilibrium, the temperature distribution in the plate

Table 2: A brief summary of numbering system convention in heat conduction according to [37, Table 2.1–2.5].

Types of boundary conditions			**Types of interface conditions**	
Notation	Name of BC	Description of BC	Notation	Description of Interface Condition
0	Zeroth kind (natural)	No physical boundary	C	Perfect contact
1	Dirichlet	Prescribed temperature	C2	Perfect contact with source at interface
2	Neumann	Prescribed heat flux	C3	Finite contact conductance
3	Robin	Convective condition	C4	Thin film at interface, perfect contact
4	Fourth kind (Carslaw)	Thin film, no convection		
5	Fifth kind (Jaeger)	Thin film, convection		
Types of time- and space-variable function at BCs				
Notation	Time-variable boundary function		Notation	Space-variable boundary function
B-	Arbitrary $f(t)$		Bx-	Arbitrary $f(x)$
B0	$f(t)=0$			
B1	$f(t)=C$			
B2	$f(t)=Ct$		Bx2	$f(x)=Cx$
B3	$f(t)=Ct^p$ with $p>1$		Bx3	$f(x)=Cx^p$ with $p>1$
B4	$f(t)=\exp(-at)$		Bx4	$f(x)=\exp(-ax)$
B5	Step changes in $f(t)$		Bx5	Step changes in $f(x)$
B6	$\sin(wt+E),\cos(wt+E)$		Bx6	$\sin(wx+E),\cos(wx+E)$
Types of space-variable initial conditions			**Types of time-variable source terms**	
Notation	Space-variable IC		Notation	Time Variation
T-	Arbitrary $F(r)$		Gt-	Arbitrary $g(t)$
T0	$F(r)=0$		Gt0	$g(t)=0$
T1	$F(r)=C$		Gt1	$g(t)=C$
T2	$F(r)=Cr$		Gt2	$g(t)=Ct$
T3	$F(r)=Cr^p$ with $p\neq 0$ or 1		Gt3	$g(t)=Ct^p$ with $p\neq 0$ or 1
T4	$F(r)=\exp(-ar)$		Gt4	$g(t)=\exp(-at)$
T5	Step changes in $F(r)$		Gt5	Step changes in $g(t)$
T6	$\sin(wr+E)$,$\cos(wr+E)$		Gt6	$\sin(wt+E)$,$\cos(wt+E)$
T7	Dirac delta function, $\delta(r-r_0)$		Gt7	Dirac delta function, $\delta(t-t_0)$

is the quadratic function [15, p. 169]

$$T(x)=T_0+(T_L-T_0)\frac{x}{L}+\frac{q'''}{2k}x(L-x). \tag{9}$$

Problem I.2 (`X11B11G0KT2`) The thermal conductivity of an infinite plate varies linearly with temperature: $k(T)=$

Table 3: Generic functional form and numbering for the quantity of interest, Q.

Types of space- and time-variable terms

Notation	Space-variable	Notation	Time-variable	Notation	Temperature-variable
Q-	Arbitrary $Q(x)$	Qt-	Arbitrary $Q(t)$	QT-	Arbitrary $Q(T)$
Q0	$Q(x) = 0$	Q0	$Q(t) = 0$	Q0	$Q(T) = 0$
Q1	$Q(x) = C$	Q1	$Q(t) = C$	Q1	$Q(T) = C$
Q2	$Q(x) = Cx$	Qt2	$Q(t) = Ct$	QT2	$Q(T) = CT$
Q3	$Q(x) = Cx^p$ with $p \neq 0$ or 1	Qt3	$Q(t) = Ct^p$ with $p \neq 0$ or 1	QT3	$Q(T) = CT^p$ with $p \neq 0$ or 1
Q4	$Q(x) = \exp(-ax)$	Qt4	$Q(t) = \exp(-at)$	QT4	$Q(T) = \exp(-aT)$
Q5	Step changes in $Q(x)$	Qt5	Step changes in $Q(t)$	QT5	Step changes in $Q(T)$
Q6	$\sin(wx+E)$, $\cos(wx+E)$	Qt6	$\sin(wt+E)$, $\cos(wt+E)$	QT6	$\sin(wT+E)$, $\cos(wT+E)$
Q7	Dirac delta function, $\delta(x-x_0)$	Qt7	Dirac delta function, $\delta(t-t_0)$	QT7	Dirac delta function, $\delta(T-T_0)$

Table 4: Verification matrix for the standard set of verification problems.

		Coordinate System			Properties and External Sources				Boundary Conditions		
	Cataloging No.	Cartesian	Cylindrical	Spherical	k	$k(T)$	q'''	$q'''(\boldsymbol{x})$	Drichlet	Neumann	Convective
I.1	`X11B11G1K1`	✓			✓		✓		✓		
I.2	`X11B11G0KT2`	✓				✓			✓		
I.3	`X21B11G1KT2`	✓				✓	✓		✓	✓	
I.4	`X23B11G1K1`	✓			✓		✓			✓	✓
I.5	`X21B11G2K1`	✓			✓			✓	✓	✓	
II.1	`R11B11G1K1`		✓		✓		✓		✓		
II.2	`R11B11G0KT2`		✓			✓			✓		
II.3	`R11B11G1KT2`		✓			✓	✓		✓		
II.4	`R23B11G1K1`		✓		✓		✓			✓	✓
II.5	`R21B01G2K1`		✓		✓			✓	✓	✓	
III.1	`RS11B11G1K1`			✓	✓		✓		✓		
III.2	`RS11B11G0KT2`			✓		✓			✓		
III.3	`RS11B11G1KT2`			✓		✓	✓		✓		
III.4	`RS23B11G1K1`			✓	✓		✓			✓	✓
III.5	`RS21B01G3K1`			✓	✓			✓	✓	✓	

$k_L + \beta(T - T_L)$, where $\beta > 0$ and $k_0 = k(T = T_0)$. It is defined on the domain $0 \leq x \leq L$, and constant temperatures are imposed on each boundary: $T(x = 0) = T_0$ and $T(x = L) = T_L$. This problem is shown schematically in Fig. 2b. The plate is

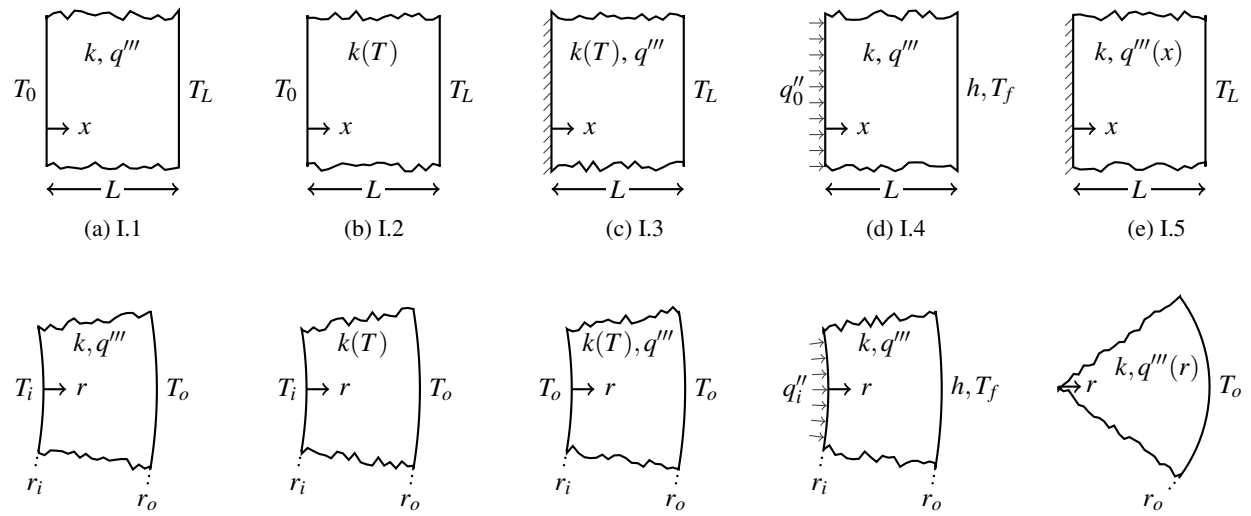

Fig. 2: Schematics showing cross sections of each of the standard verification problems. The first row are problems in Cartesian coordinates and second row are problems in curvilinear (i.e., cylindrical and spherical) coordinates.

allowed to reach thermal equilibrium, and the analytic solution for the temperature distribution is [15, p. 138]

$$T(x) = T_L + \frac{k_L}{\beta}\left[\sqrt{1+\beta\frac{(k_0+k_L)}{k_L^2}\frac{(L-x)}{L}(T_0-T_L)}-1\right]. \tag{10}$$

Problem I.3 (`X21B11G1KT2`) The thermal conductivity of an infinite plate varies linearly with temperature: $k(T) = k_o(1+\beta T)$, where $\beta > 0$ and k_o is an arbitrary constant. It is defined on the domain $0 \le x \le L$, has a constant internal heat generation q''', and has the boundary conditions $dT/dx\big|_{x=0} = 0$ and $T(x=L) = T_L$. A schematic of this problem is shown in Fig. 2c. The plate is allowed to reach thermal equilibrium, and the analytic solution for the temperature distribution is [38, pp. 129–132]

$$T(x) = T_L + \frac{1}{\beta}\left[\sqrt{1+\left(\frac{\beta q''' L^2}{k_o}\right)\left(1-\frac{x^2}{L^2}\right)}-1\right]. \tag{11}$$

Problem I.4 (`X23B11G1K1`) An infinite plate with constant thermal conductivity k and internal heat generation q''' is defined on the domain $0 \le x \le L$. The left boundary has an imposed constant heat flux $-kdT/dx\big|_{x=0} = q''_0$. The right boundary is exposed to a fluid with constant temperature T_f and heat transfer coefficient h, which results in the convective boundary condition $-kdT/dx\big|_{x=L} = h(T-T_f)$. A schematic of this problem is shown in Fig. 2d. Under thermal equilibrium, the temperature distribution in the plate is

$$T(x) = T_f + q''_0\left(\frac{L-x}{k}+\frac{1}{h}\right) + q'''\left(\frac{L^2-x^2}{2k}+\frac{L}{h}\right). \tag{12}$$

Problem I.5 (`X21B11G2K1`) The volumetric heat generation in an infinite plate varies linearly with spatial location $q'''(x) = q'''_o(1-\beta x/L)$ in the domain $0 \le x \le L$. The plate has constant thermal conductivity k. It is insulated on the left boundary and has a constant temperature imposed on the right: $-kdT/dx\big|_{x=0} = 0$ and $T(x=L) = T_L$. A schematic of this problem is shown in Fig. 2e. The plate is allowed to reach thermal equilibrium, and the analytic solution for the temperature distribution is

$$T(x) = T_L + \frac{q'''_o L^2}{2k}\left[1-\frac{x^2}{L^2}-\frac{\beta}{3}\left(1-\frac{x^3}{L^3}\right)\right]. \tag{13}$$

4.2 Cylindrical Coordinates

Problem II.1 (R11B11G1K1) An infinitely long hollow cylinder has an inner radius r_i and an outer radius r_o, where $0 < r_i \leq r \leq r_o$. It has a constant thermal conductivity k and constant internal heat generation q'''. It is allowed to reach thermal equilibrium and has constant temperatures imposed on its inside and outside boundaries: $T(r = r_i) = T_i$ and $T(r = r_o) = T_o$. A schematic of this problem is shown in Fig. 2f. The analytical solution for the temperature distribution is

$$T(r) = \frac{1}{\ln(\frac{r_i}{r_o})} \left\{ T_o \ln(r_i) - T_i \ln(r_o) + (T_i - T_o)\ln(r) + \frac{q'''}{4k} \left[r_o^2 \ln\left(\frac{r_i}{r}\right) + r_i^2 \ln\left(\frac{r}{r_o}\right) + r^2 \ln\left(\frac{r_o}{r_i}\right) \right] \right\}. \tag{14}$$

Problem II.2 (R11B11G0KT2) The thermal conductivity of an infinitely long hollow tube varies linearly with temperature: $k(T) = k_o + \beta(T - T_o)$, where $\beta > 0$ and $k_i = k(T = T_i)$. The tube's inside radius is r_i and outside radius is r_o, where $0 < r_i \leq r \leq r_o$. The inner and outer surfaces have imposed constant temperatures $T(r = r_i) = T_i$ and $T(r = r_o) = T_o$. A schematic of this problem is shown in Fig. 2g. In thermal equilibrium, the analytic solution for the temperature distribution is [15, p. 138]

$$T(r) = T_o + \frac{k_o}{\beta} \left[\sqrt{1 + \beta \frac{(k_i + k_o)}{k_o^2} \frac{\ln(r/r_o)}{\ln(r_i/r_o)} (T_i - T_o)} - 1 \right]. \tag{15}$$

Problem II.3 (R11B11G1KT2) The thermal conductivity of an infinitely long hollow cylinder varies linearly with temperature: $k(T) = k_0(1 + \beta T)$, where $\beta > 0$ and k_0 is an arbitrary constant. The tube's inside radius is r_i and outside radius is r_o, where $0 < r_i \leq r \leq r_o$. It has a constant internal heat generation q''' and has the same constant temperature imposed on both surfaces: $T(r = r_i) = T(r = r_o) = T_o$. A schematic of this problem is shown in Fig. 2h. If the cylinder reaches thermal equilibrium, the analytic solution for the temperature distribution is [39, p. 194]

$$T(r) = T_o + \frac{1}{\beta} \left\{ \sqrt{1 + \frac{q'''\beta}{2k_0} \left[(r_o^2 - r^2) - \frac{(r_o^2 - r_i^2)}{\ln(r_o/r_i)} \ln\left(\frac{r_o}{r}\right) \right]} - 1 \right\}. \tag{16}$$

Problem II.4 (R23B11G1K1) An infinitely long hollow cylinder has thermal conductivity k and internal heat generation q'''. Its inner radius is r_i and outer radius is r_o, where $0 < r_i \leq r \leq r_o$. A constant heat flux is applied to the inside surface $-kdT/dr\big|_{r=r_i} = q_i''$, and the outside surface is exposed to a fluid temperature T_f and heat transfer coefficient h, which results in the convective boundary condition $-kdT/dr\big|_{r=r_o} = h(T - T_f)$. A schematic of this problem is shown in Fig. 2i. If the cylinder is in thermal equilibrium, the analytic solution for the temperature distribution is [11, pp. 2-33]

$$T(r) = T_f + \frac{q'''}{4k} \left[\frac{2k}{hr_o} \left(r_o^2 - r_i^2\right) + r_o^2 - r^2 + 2r_i^2 \ln\left(\frac{r}{r_o}\right) \right] + \frac{q_i'' r_i}{k} \left[\frac{k}{hr_o} - \ln\left(\frac{r}{r_o}\right) \right]. \tag{17}$$

Problem II.5 (R21B01G2K1) The volumetric heat generation in an infinitely long solid cylinder varies with spatial location $q'''(r) = q_o'''(1 - \beta r/r_o)$. The radius of the cylinder is r_o, where $0 \leq r \leq r_o$, and it has a constant thermal conductivity k. A constant temperature is imposed on its surface $T(r = r_o) = T_o$. A schematic of this problem is shown in Fig. 2j. Under thermal equilibrium, the temperature distribution in the cylinder is

$$T(r) = T_o + \frac{q_o''' r_o^2}{4k} \left[\left(1 - \frac{r^2}{r_o^2}\right) - \frac{4\beta}{9} \left(1 - \frac{r^3}{r_o^3}\right) \right]. \tag{18}$$

4.3 Spherical Coordinates

Problem III.1 (RS11B11G1K1) A spherical shell has a constant thermal conductivity k and internal heat generation q'''. It has inner radius r_i and outer radius r_o, where $0 < r_i \leq r \leq r_o$. Both surfaces have constant temperatures imposed: $T(r = r_i) = T_i$ and $T(r = r_o) = T_o$. A schematic of this problem is shown in Fig. 2f. If the spherical shell is in thermal

equilibrium, the analytic solution for the temperature distribution is [15, p. 136]

$$T(r) = \frac{1}{\left(\frac{1}{r_i} - \frac{1}{r_o}\right)} \left[T_o \left(\frac{1}{r_i} - \frac{1}{r} \right) - T_i \left(\frac{1}{r_o} - \frac{1}{r} \right) \right] - \frac{q'''}{6kr} (r - r_i)(r - r_o)(r + r_i + r_o). \tag{19}$$

Problem III.2 (RS11B11G0KT2) A spherical shell has a thermal conductivity that varies linearly with temperature: $k(T) = k_o + \beta(T - T_o)$, where $\beta > 0$ and $k_o = k(T = T_o)$. It has an inside radius r_i and outside radius r_o, where $0 < r_i \leq r \leq r_o$. The inside and outside surfaces have imposed constant temperatures: $T(r = r_i) = T_i$ and $T(r = r_o) = T_o$. A schematic of this problem is shown in Fig. 2g. In thermal equilibrium, the analytic solution for the temperature distribution is [15, p. 139]

$$T(r) = T_o + \frac{k_o}{\beta} \left[\sqrt{1 + \beta \frac{(k_i + k_o)}{k_o^2} \frac{\left(\frac{1}{r} - \frac{1}{r_o}\right)}{\left(\frac{1}{r_i} - \frac{1}{r_o}\right)} (T_i - T_o)} - 1 \right]. \tag{20}$$

Problem III.3 (RS11B11G1KT2) The thermal conductivity of a spherical shell varies linearly with temperature: $k = k_0(1 + \beta T)$, where $\beta > 0$ and k_0 is an arbitrary constant. The inside radius is r_i and the outside radius is r_o, where $0 < r_i \leq r \leq r_o$. It has a constant internal heat generation q''', and the same constant temperature is imposed on both surfaces: $T(r = r_i) = T(r = r_o) = T_o$. A schematic of this problem is shown in Fig. 2h. In thermal equilibrium, the analytic solution for the temperature distribution is

$$T(r) = T_o + \frac{1}{\beta} \left\{ \sqrt{1 + \frac{q'''\beta}{3k_0} \left[(r_o^2 - r^2) - (r_o^2 - r_i^2) \frac{\left(\frac{1}{r} - \frac{1}{r_o}\right)}{\left(\frac{1}{r_i} - \frac{1}{r_o}\right)} \right]} - 1 \right\}. \tag{21}$$

Problem III.4 (RS23B11G1K1) A spherical shell has thermal conductivity k and heat generation q'''. It has an inner radius r_i and an outer radius r_o, where $0 < r_i \leq r \leq r_o$. A constant heat flux is applied to the inside surface $-kdT/dr\big|_{r=r_i} = q_i''$ and the outside surface is exposed to a fluid temperature T_f and heat transfer coefficient h, which results in the convective boundary condition $-kdT/dr\big|_{r=r_o} = h(T - T_f)$. A schematic of this problem is shown in Fig. 2i. In thermal equilibrium, the analytic solution for the temperature distribution is

$$T(r) = T_f + \frac{q'''}{6k} \left[r_o^2 - r^2 + \frac{2k}{hr_o^2}(r_o^3 - r_i^3) + 2r_i^3 \left(\frac{1}{r_o} - \frac{1}{r} \right) \right] + \frac{q_i'' r_i^2}{k} \left[\frac{1}{r} - \frac{1}{r_o} + \frac{k}{hr_o^2} \right]. \tag{22}$$

Problem III.5 (RS21B01G3K1) A solid sphere has a spatially dependent internal heating $q''' = q_o''' \left(1 - \beta r^2/r_o^2\right)$. The radius of the sphere is r_o, where $0 \leq r \leq r_o$, and it has a constant thermal conductivity k. It has a constant temperature imposed on its boundary $T(r = r_o) = T_o$. A schematic of this problem is shown in Fig. 2j. The sphere reaches thermal equilibrium, and the analytic solution for the temperature distribution is [11, 40]

$$T(r) = T_o + \frac{q_o''' r_o^2}{6k} \left[\left(1 - \frac{r^2}{r_o^2} \right) - \frac{3\beta}{10} \left(1 - \frac{r^4}{r_o^4} \right) \right]. \tag{23}$$

5 Example Verification of a Finite Element Code

The code verification procedure described previously is applied here to an M&S tool that simulates the thermo-mechanical behavior of nuclear fuel, which is an important component of nuclear reactor analysis. In normal operating conditions, the fuel melting temperature imposes limits on the total power output of a reactor, so a full characterization of the temperature distribution within the fuel is important. This requires an understanding of the thermal behavior of the fuel, gap filled with inert gas, the cladding material that encloses the nuclear fuel, and any deposits that may exist on the surface of the cladding. Fuel behavior is also consequential to the modeling of severe accident scenarios, as the cladding serves as the first barrier that prevents releases of radioactive material. As such, cladding temperature, creep, swelling, and rupture are included as

modeling requirements for testing of light-water reactor (LWR) emergency core cooling system [41]. As fuel modeling is important and consequential, it is necessary to ensure the predictive capability of relevant simulation codes. There are a variety of codes that approximate the fuel behavior [42, 43, 32, 44, 45, 46, 47], and all of them include a conduction solution. In this demonstration, the nuclear fuel performance code BISON [6] is analyzed.

BISON is an advanced nuclear fuel performance code that uses the FEM to model the thermo-mechanical behavior of nuclear fuel using high-performance M&S. BISON solves the fully-coupled equations of energy conservation, mechanics, and species conservation to account for a majority of possible fuel behaviors. It is capable of modeling fuel plates, fuel rods, and tri-structural isotropic (TRISO) fuel particles. It can employ three-dimensional Cartesian, two-dimensional axisymmetric cylindrical, or one-dimensional radial spherical geometry. It includes empirical models for a wide variety of fuel physics: thermal properties dependent upon temperature and fuel utilization; fuel swelling, fracture, and densification; fission gas production; cladding creep and plasticity; and models for both the lateral and axial gap between the fuel and cladding material. Because of the plate, cylindrical, and spherical geometries of the fuel forms modeled by BISON, the verification problems discussed here are of particular interest for these applications.

In this section, the use of three of the code verification problems from Section 4 is shown for code verification of BISON. Only this small subset of verification problems is shown here for brevity. The verification is straightforward for each problem. More details for each of these problems, as well as other problems, can be found in the technical report [9]. It should be noted that the capabilities tested here are actually all fully provided by the common physics models provided by the MOOSE framework, so these tests serve to verify any MOOSE-based code that uses those models, in addition to BISON.

In these examples, the BISON models are all one-dimensional. In general, though, the proposed set of problems could also be run in higher dimensions, which would add additional sets of rows and columns to the matrix in Table 4. The set of plate problems (I.1-I.5) can be run on one-, two-, or three-dimensional meshes with Cartesian coordinates. The cylinder problems (II.1-II.5) can be run with one- or two-dimensional meshes with axisymmetric coordinates, or with two- or three-dimensional meshes with Cartesian coordinates. The spherical problems (III.1-III.5) can be run with a one-dimensional mesh with spherical coordinates, a two-dimensional mesh with axisymmetric coordinates, or a three-dimensional mesh with Cartesian coordinates. Including all of these cases would result in expanding the test matrix from 15 problems to 50 problems. For brevity, only the one-dimensional cases are shown here, but these can easily be expanded to higher-dimensional problems.

5.1 Infinite plate with temperature dependent thermal conductivity (Problem I.2, Fig. 2b).

The problem is run in BISON on the domain $\boldsymbol{X} \in [0,1]$ with the Dirichlet boundary conditions $T_0 = 300\,\mathrm{K}$ and $T_L = 0\,\mathrm{K}$. Steady state heat conduction is considered using a temperature-dependent thermal conductivity, where $k_L = 5\,\mathrm{W/m/K}$. The degree of nonlinearity of the heat conduction equation is determined by β, and two cases are examined here: $\beta = 0.001$ and $\beta = 0.1$. The results for the cases are shown respectively in Fig. 3 and Fig. 4.

The top row of the set of figures for each problem shows the exact and computed solution for three different meshes. Both linear and quadratic FE types are simulated. The next row indicates the difference between the computed solution and the exact solution; the difference at the finite element edges are indicated as points, whereas the error inside the elements is indicated by the filled area. Finally, for each problem, the results of a convergence study, which was conducted with a spatial refinement factor of two ($r_x = 2$), are shown. The computed norms for the two element types are shown as a function of mesh size h. All results match with the expected behavior discussed in Section 2. Norms are shown in the difference between the computed and exact solution for both temperature (solid lines) and heat flux (dashed lines). The formal orders of accuracy for all cases were derived in Appendix A. For linear FE, the formal order is two for temperature and one for heat flux. For quadratic FE, the formal order is three for temperature and two for heat flux. In the asymptotic region, all errors converge to the exact solution with the correct order of accuracy.

5.2 Hollow cylinder with internal heating and outside convection boundary (Problem II.4, Fig. 2i).

The problem is solved in BISON on the domain $\boldsymbol{X} \in [0.2, 1.0]$, with an insulated inside boundary and a convective outside boundary. The fluid temperature and heat transfer coefficient are $T_f = 100\,\mathrm{K}$ and $h = 10\,\mathrm{W/m^2/K}$. The constant thermal conductivity is $k = 1\,\mathrm{W/m/K}$, and the volumetric heat generation is $q''' = 1200\,\mathrm{W/m^3}$. The results are shown in Fig. 5, which has the same information and format as discussed in Section 5.1. The behavior of the numerical error with respect to mesh spacing matches with the discussion in Section 2. In the asymptotic region, all errors converge to the exact solution with the correct order of accuracy.

5.3 Solid sphere with spatially varying internal heating (Problem III.5, Fig. 2j)

A BISON input is formulated to run this problem on the domain $\boldsymbol{X} \in [0,1]$ with a Dirichlet outside boundary $T_o = 300\,\mathrm{K}$. Steady state heat conduction is considered in the sphere with constant thermal conductivity $k = 1\,\mathrm{W/m/K}$. The results shown in Fig. 6 are in the same format as previous sections. The behavior of the numerical error with respect to mesh spacing matches with the discussion in Section 2. In the asymptotic region, all errors converge to the exact solution with the correct

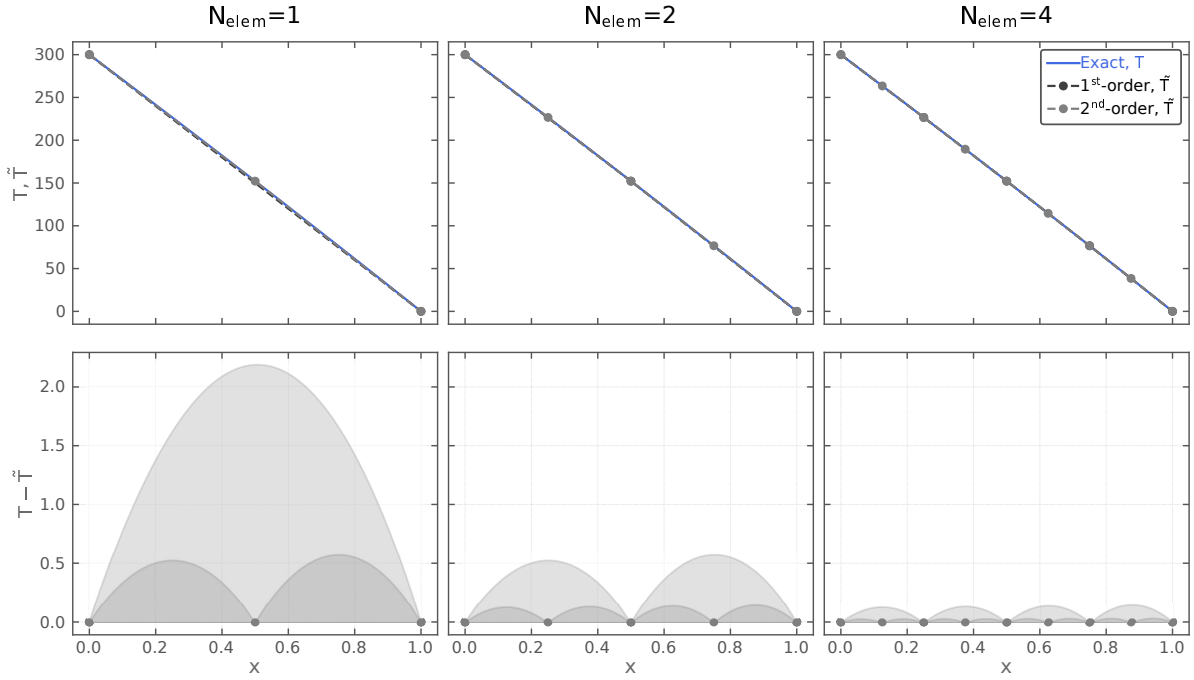

(a) Temperature distribution for the the first three meshes using one-dimensional elements. *First row*: exact and numerical solutions. *Second row*: difference between the exact and computed solutions.

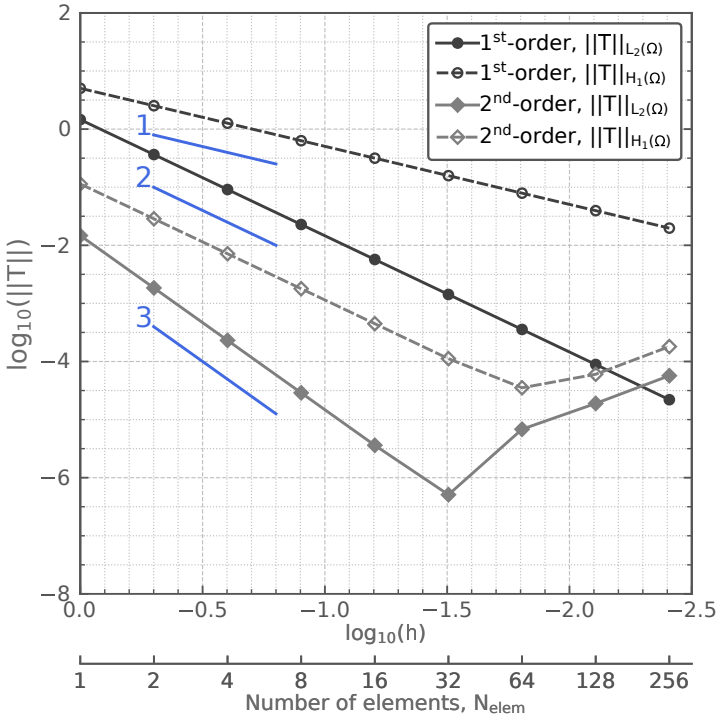

(b) Spatial refinement analysis ($r_x = 2$). *Solid lines*: the L_2-norm quantifies convergence of the temperature distribution. *Dashed lines*: the H_1-norm quantifies convergence of the heat flux. Slopes of first-, second-, and third-order convergence are indicated.

Fig. 3: BISON results for Problem I.2 (`X11B11G0KT2`) with $\beta = 0.001$.

order of accuracy.

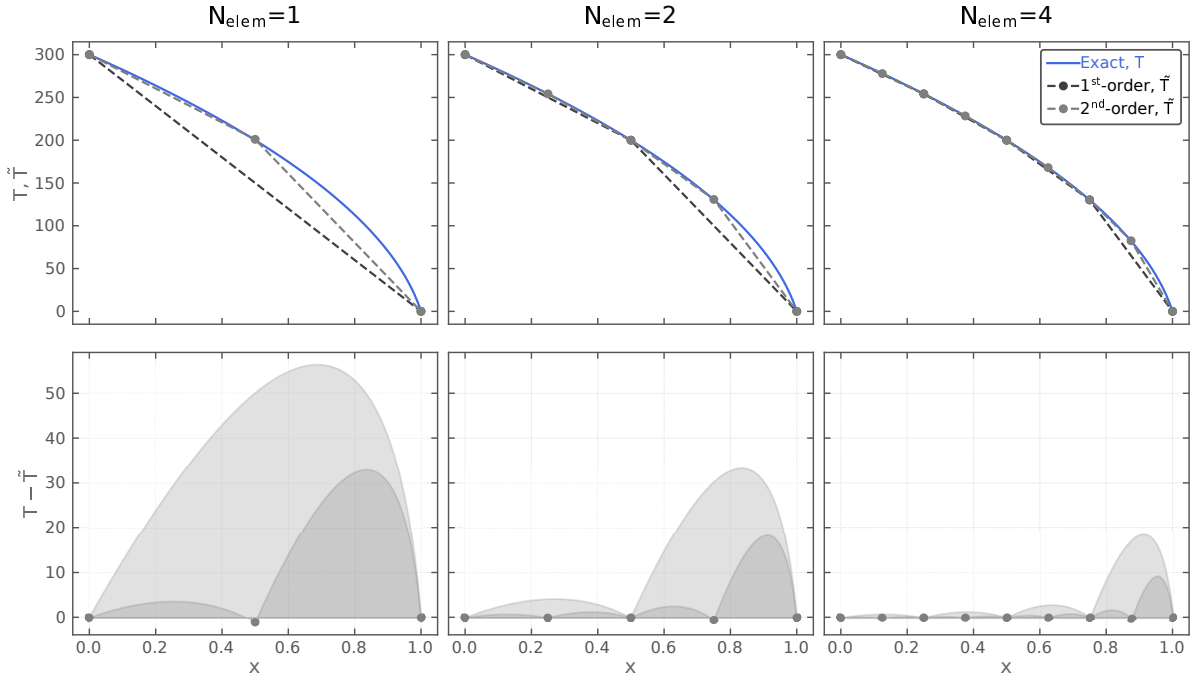

(a) Temperature distribution for the the first three meshes using one-dimensional elements. *First row*: exact and numerical solutions. *Second row*: difference between the exact and computed solutions.

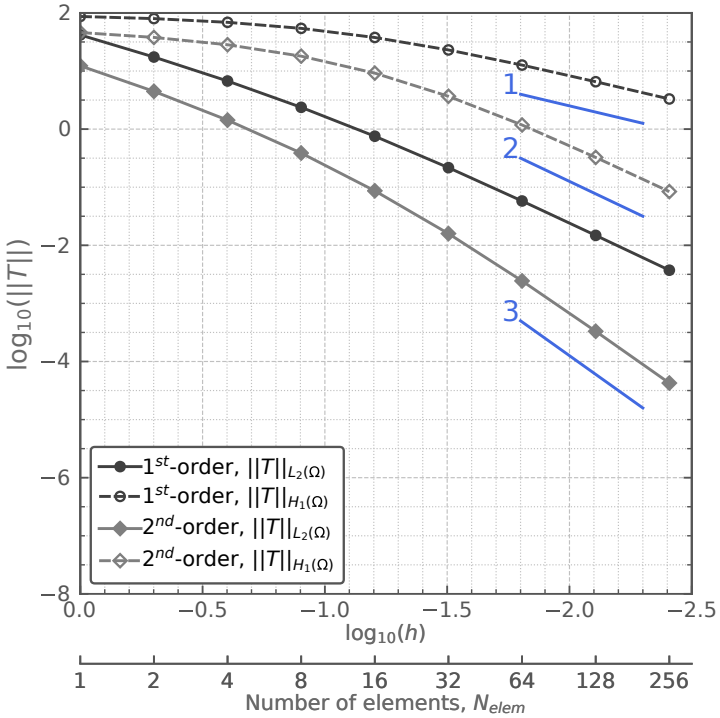

(b) Spatial refinement analysis ($r_x = 2$). *Solid lines*: the L_2-norm quantifies convergence of the temperature distribution. *Dashed lines*: the H_1-norm quantifies convergence of the heat flux. Slopes of first-, second-, and third-order convergence are indicated.

Fig. 4: BISON results for Problem I.2 (`X11B11G0KT2`) with $\beta = 0.1$.

6 Conclusion

Code verification exercises are helpful to ensure the correct implementation of numerical methods that use discretization to solve differential or integral equations. This process quantifies whether an M&S tool converges to the correct answer at

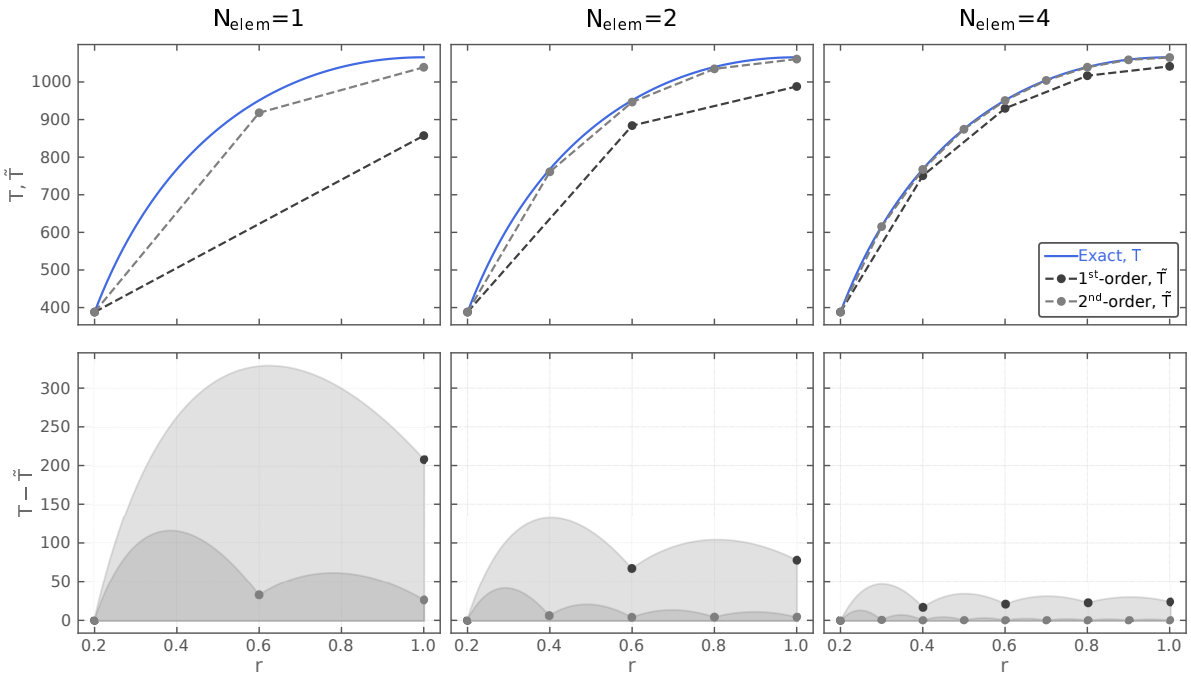

(a) Temperature distribution for the the first three meshes using one-dimensional elements. *First row*: exact and numerical solutions. *Second row*: difference between the exact and computed solutions.

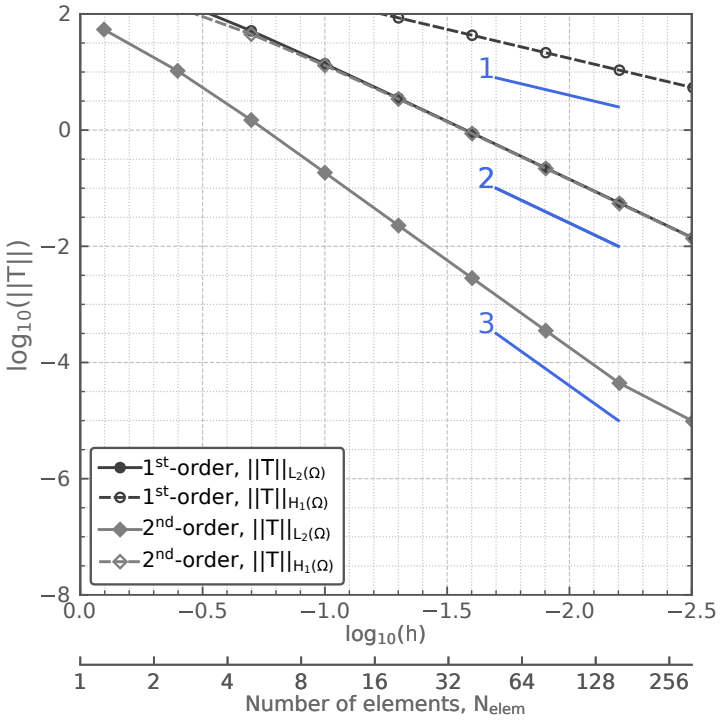

(b) Spatial refinement analysis ($r_x = 2$). *Solid lines*: the L_2-norm quantifies convergence of the temperature distribution. *Dashed lines*: the H_1-norm quantifies convergence of the heat flux. Slopes of first-, second-, and third-order convergence are indicated.

Fig. 5: BISON results for Problem II.4 (`R23B11G1K1`).

the theoretical rate for a particular problem. Any simulation tool with a thorough verification pedigree is likely to be accurate and free of coding mistakes. In this study, a physics-based process for defining a code verification matrix was demonstrated. The process involved defining a problem of interest, mapping all code capabilities to a matrix, and then selecting specific reference problems to fill the matrix. This process is intended to provide sufficient code verification evidence without

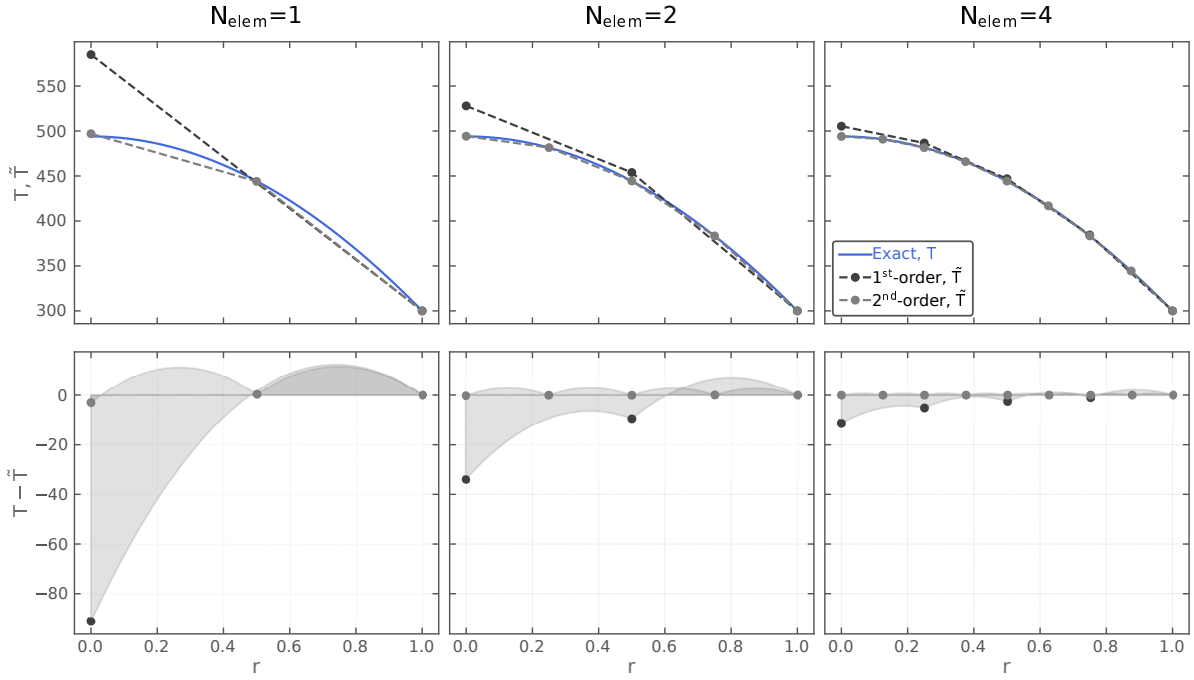

(a) Temperature distribution for the the first three meshes. *First row*: exact and numerical solutions. *Second row*: difference between the exact and computed solutions.

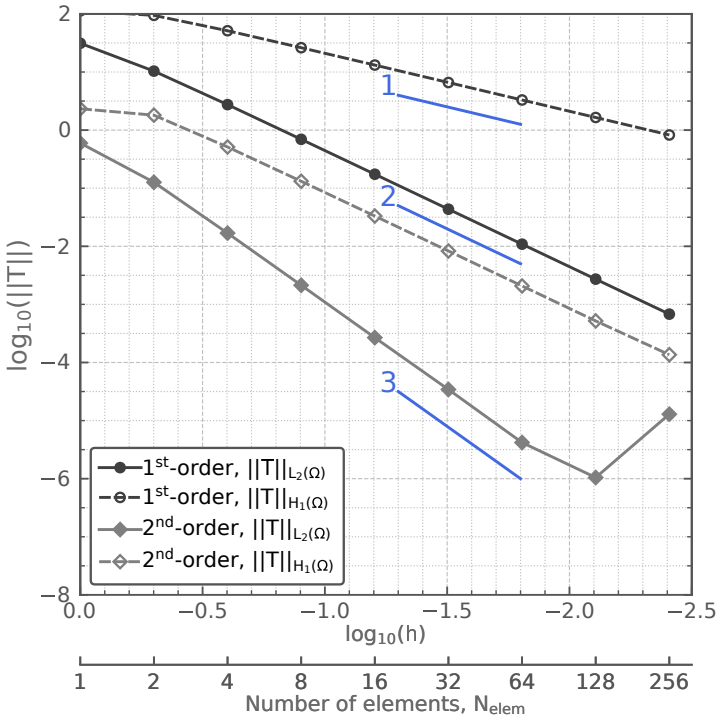

(b) Spatial refinement analysis ($r_r = 2$). *Solid lines*: the L_2-norm quantifies convergence of the temperature distribution. *Dashed lines*: the H_1-norm quantifies convergence of the heat flux. Slopes of first-, second-, and third-order convergence are indicated.

Fig. 6: BISON results for Problem III.5 (`RS21B01G3K1`).

performing unnecessary or redundant work. By mapping code capabilities this way, it is ensured that the full pedigree of a code is accessible and clear and that gaps in testing are easy to identify and address.

The capabilities considered in this work included the coordinate system, treatment of the thermal conductivity, treatment of the external heat source, and boundary conditions. The fifteen problems were chosen such that there were five problems

for each coordinate system that tested similar simulation options. All simulation options were tested by at least one problem, and most combinations of simulations were also tested by these problems. Although the demonstration included in this work—fifteen one-dimensional steady state solutions to the conduction equation—is relatively simple, it can be easily expanded. As previously mentioned, this set of problems can also be expanded to include multi-dimensional variants. Also, transient problems and tests of application-specific empirical models can be added. In addition, this physics-based process for construction of a verification matrix can be applied to other conservation equations of interest.

After the verification matrix was constructed, the BISON nuclear fuel performance code was used to demonstrate the verification procedure for the established problems. All verification problems display the proper convergence behavior for both first- and second-order FEs: (1) second-order convergence of the temperature and first-order convergence of the heat flux for linear FEs and (2) third-order convergence of the temperature and second-order convergence of the heat flux for quadratic FEs. The correct order of accuracy is observed in the asymptotic region, but, eventually, numerical error dominates the solution (see Fig. 1) as higher order LTE terms degrade the solution. The results provide supporting evidence that the BISON solution is a faithful representation of the underlying mathematical model.

The problems in this study use simple meshes and uniform mesh refinement. This creates a strong base of verification, but future work may expand to more complicated refinement strategies: more complex meshes, non-uniform mesh refinement, local mesh refinement, differing aspect ratios, and combined temporal-spatial order analysis. Specific to the BISON code, future work will include the verification of (1) solid mechanics, (2) species diffusion, (3) multiphysics coupling, as well as (4) the expansion of heat conduction problems to transients and multi-dimensional domains. Significant effort is required to expand the verification matrix to include two- and three-dimensional problems, problems with atypical behavior, and problems that couple more than one conservation equation. This could reveal coding errors that are hidden when only individual equations are tested.

Acknowledgements

Thanks to Aaron Krueger of Sandia National Laboratories (SNL) for his technical review of this work. Sandia National Laboratories is a multimission laboratory managed and operated by National Technology & Engineering Solutions of Sandia, LLC, a wholly-owned subsidiary of Honeywell International Inc., for the U.S. Department of Energy's National Nuclear Security Administration under contract DE-NA0003525. This research is supported by and performed in conjunction with the Consortium for Advanced Simulation of Light Water Reactors (`http://www.casl.gov`), an Energy Innovation Hub (`http://www.energy.gov/hubs`) for Modeling and Simulation of Nuclear Reactors under US Department of Energy Contract No. DE-AC05-00OR22725. Any subjective views or opinions that might be expressed in the paper do not necessarily represent the views of the U.S. Department of Energy or the United States Government.

References

[1] Oberkampf, W. L., and Roy, C. J., 2010. *Verification and Validation in Scientific Computing*, first ed. Cambridge University Press, Cambridge, UK, 11.

[2] Salari, K., and Knupp, P., 2000. Code verification by the method of manufactured solutions. Tech. Rep. SAND2000-1444, SNL, 6.

[3] Oberkampf, W. L., Pilch, M., and Trucano, T. G., 2007. Predictive capability maturity model for computational modeling and simulation. Tech. Rep. SAND2007-5948, SNL.

[4] Roache, P. J., 1998. *Verification and Validation in Computational Science and Engineering*. Hermosa Publishing, Albuquerque, NM.

[5] Williamson, R. L., et al., 2012. "Multidimensional multiphysics simulation of nuclear fuel behavior". *Journal of Nuclear Materials,* **423**(1–3), pp. 149–163.

[6] Hales, J. D., et al., 2014. *BISON Theory Manual The Equations Behind Nuclear Fuel Analysis*. INL, Idaho Falls, Idaho, 10.

[7] Williamson, R. L., Hales, J. D., et al., 2020. "BISON: A flexible code for advanced simulation of the performance of multiple nuclear fuel forms". *Nuclear Technology*. (*accepted for publication*).

[8] Permann, C. J., Gaston, D. R., Andrš, D., Carlsen, R. W., Kong, F., Lindsay, A. D., Miller, J. M., Peterson, J. W., Slaughter, A. E., Stogner, R. H., and Martineau, R. C., 2020. "MOOSE: Enabling massively parallel multiphysics simulation". *SoftwareX,* **11**, p. 100430.

[9] Toptan, A., Porter, N. W., Hales, J. D., Williamson, R. L., and Pilch, M., 2020. FY20 verification of BISON using analytic and manufactured solutions. Tech. Rep. CASL-U-2020-1939-000; SAND2020-3887R, Consortium for Advanced Simulation of LWRs (CASL), 3.

[10] McHale, M. P., et al., 2009. Standard for verification and validation in computational fluid dynamics and heat transfer. Standard ASME V&V 20-2009, American Society of Mechanical Engineers (ASME).

[11] VanSant, J. H., 1983. Conduction heat transfer solutions. Tech. Rep. UCRL—52863-Rev.l; DE87 012387, Lawrence Livermore National Lab., 8.
[12] Cole, K. D., et al., 2014. "Intrinsic verification and a heat conduction database". *International Journal of Thermal Sciences,* **78**, pp. 36–47.
[13] Exact Analytical Conduction Toolbox (EXACT), 2019. University of Nebraska–Lincoln. `https://exact.unl.edu/exact/home/home.php`.
[14] Carslaw, H. S., and Jaeger, J. C., 1959. *Conduction of Heat in Solids*, 2nd ed. Oxford at The Clarendon Press.
[15] Jakob, M., 1949. *Heat transfer*, Vol. 1. Wiley, New York, NY.
[16] Hahn, D. W., and Ozisik, M. N., 2012. *Heat Conduction*, 3rd ed. John Wiley & Sons, Inc., Hoboken, NJ.
[17] Beck, J., Haji-Sheikh, A., and Amos, D., 2004. "Verification solution for partial heating of rectangular solids". *Int J. Heat Mass Trans,* **47**(19-20), pp. 4243 – 4255.
[18] McMasters, R., Zhou, Z., and Dowding, K., 2002. "Exact solution for nonlinear thermal diffusion and its use for verification". *J. Thermophysics and Heat Trans.,* **16**(3), pp. 366 – 372.
[19] McMasters, R., Dowding, K., and Beck, J., 2002. "Methodology to generate accurate solutions for verification in transient three-dimensional heat conduction". *Numerical Heat Transfer, Part B: Fundamentals,* **41**(6), pp. 521–541.
[20] McMasters, R., de Monte, F., and Beck, J. V., 2019. "Generalized solution for two-dimensional transient heat conduction problems with partial heating near a corner". *ASME Journal of Heat Transfer,* **141**(7), pp. 071301 – 071308.
[21] McMasters, R., de Monte, F., and Beck, J. V., 2020. "Generalized solution for rectangular three-dimensional transient heat conduction problems with partial heating". *Journal of Thermophysics and Heat Transfer (AIAA),* **34**(3), pp. 516 – 521.
[22] Hirt, C. W., 1968. "Heuristic stability theory for finite-difference equations". *Journal of Computational Physics,* **2**, pp. 339–355.
[23] Grinstein, F. F., Margolin, L. G., and Rider, W. J., 2007. *Implicit Large Eddy Simulation: Computing Turbulent Fluid Dynamics*. Cambridge University Press, Cambridge, UK.
[24] Porter, N. W., Salko, R. K., and Pilch, M., 2020. FY20 improvements to CTF code verification and unit testing. Tech. Rep. SAND2020-2719R; CASL-U-2020-1938-000, CASL.
[25] Pfefferer, J., and Winkler, M., 2018. "Finite element error estimates for normal derivatives on boundary concentrated meshes". *SIAM Journal on Numerical Analysis,* **57**(5), pp. 2043–2073.
[26] Banks, J. W., Aslam, T., and Rider, W. J., 2008. "On sub-linear convergence for linearly degenerate waves in capturing schemes". *Journal of Computational Physics,* **227**, pp. 6985–7002.
[27] Kamm, J., Rider, W., and Brock, J., 2003-4041. "Combined space and time convergence analysis of a compressible flow algorithm". *AIAA Paper*.
[28] Burnett, D. S., 1987. *Finite Element Analysis from Concepts to Applications*. Addison-Wesley Publishing Company, Reading, MA.
[29] Ross, A. M., and Stoute, R. L., 1962. Heat transfer coefficient between UO_2 and Zircaloy-2. Tech. Rep. AECL-1552, Atomic Energy of Canada Limited.
[30] Lanning, D. D., and Hann, C. R., 1975. Review of methods applicable to the calculation of gap conductance in zircaloy-clad UO_2 fuel rods. Tech. Rep. BWNL-1894, UC-78B, Pacific Northwest National Laboratory.
[31] Allison, C. M., et al., 1993. SCDAP/RELAP5/MOD3.1 code manual, volume IV: MATPRO–A library of materials properties for light-water-reactor accident analysis. Tech. Rep. NUREG/CR-6150, EGG-2720, Idaho National Engineering Laboratory.
[32] Toptan, A., Salko, R. K., Avramova, M. N., Clarno, K., and Kropaczek, D. J., 2019. "A new fuel modeling capability, CTFFuel, with a case study on the fuel thermal conductivity degradation". *Journal of Nuclear Engineering and Design,* **341**, pp. 248–258.
[33] Toptan, A., Kropaczek, D. J., and Avramova, M. N., 2019. "Gap conductance modeling I: Theoretical considerations for single- and multi-component gases in curvilinear coordinates". *Nuclear Engineering and Design,* **353**, p. 110283.
[34] Toptan, A., Kropaczek, D. J., and Avramova, M. N., 2019. "Gap conductance modeling II: Optimized model for UO_2-Zircaloy interfaces". *Nuclear Engineering and Design,* **355**, p. 110289.
[35] Toptan, A., Hales, J. D., Williamson, R. L., Novascone, S. R., Pastore, G., and Kropaczek, D. J., 2020. "Modeling of gap conductance for LWR fuel rods applied in the BISON code". *Journal of Nuclear Science and Technology,* **57**(8), pp. 963–974.
[36] Beck, J. V., and Litkouhi, B., 1985. Heat conduction numbering system. ASME paper 85-WA/HT-63, ASME.
[37] Cole, K. D., 2011. *Heat conduction using Green's functions*. CRC Press, Boca Raton.
[38] Arpaci, V. S., 1966. *Conduction Heat Transfer*. Addison-Wesley Publishing Company, Reading, MA.
[39] Scheider, P. J., 1955. *Conduction Heat Transfer*. Addison-Wesley Publishing Company, Inc., Cambridge, MA.
[40] Bird, R. B., Stewart, W. E., and Lightfoot, E. N., 1960. *Transport Phenomena*. John Wiley & Sons, Inc., New York, New York.
[41] Nuclear Regulatory Commission. 10 CFR Part 50: Domestic Licensing of Production and Utilization Facilities.

https://www.nrc.gov/reading-rm/doc-collections/cfr/part050/.
[42] U. S. Nuclear Regulatory Commission, 2015. TRACE V5.0 Theory Manual: Field Equations, Solution Methods, and Physical Models.
[43] Salko, R., et al., 2019. CTF 4.0 theory manual. Tech. Rep. ORNL/TM-2019/1145, Oak Ridge National Lab. (ORNL), Oak Ridge, TN, 4.
[44] Porter, N., Mousseau, V., and Avramova, M., 2019. "CTF-R: A novel residual-based thermal hydraulic solver". *Nuclear Engineering and Design,* **348**, July, pp. 37–45.
[45] Electric Power Research Institute, 2004. Fuel Analysis and Licensing Code: FALCON MOD01: Volume 1: Theoretical and Numerical Bases, 12.
[46] Geelhood, K. J., Luscher, W. G., Raynaud, P. A., and Porter, I. E., 2015. FRAPCON-4.0: A computer code for the calculation of steady-state, thermal-mechanical behavior of oxide fuel rods for high burnup. Tech. Rep. PNNL-19418, Vol.1 Rev.2, PNNL.
[47] Geelhood, K. J., Luscher, W. G., Raynaud, P. A., and Porter, I. E., 2016. Fraptran-2.0: A computer code for the transient analysis of oxide fuel rods. Tech. Rep. PNNL-19400, Vol.1 Rev2, Pacific Northwest National Laboratory, Richland, WA, 5.
[48] Zienkiewicz, O. C., Taylor, R. L., and Zhu, J. Z., 2013. *The Finite Element Method Its Basis & Fundamentals*. Elsevier, New York, NY.
[49] Oliveira, E. R. D. A. E., 1968. "Theoretical foundations of the finite element method". *International Journal of Solids and Structures,* **4**(10), 10, pp. 929–952.
[50] Aziz, A. K., 1972. *The Mathematical Foundations of The Finite Element Method with Applications to Partial Differential Equations*. Academic Press, New York, NY.
[51] Oden, J. T., and Reddy, J. N., 1976. *An Introduction to the Mathematical Theory of Finite Elements*. John Wiley & Sons, New York, NY.
[52] Babuska, I., and Szabo, B., 1982. "On the rates of convergence of the finite element method". *International Journal for Numerical Methods in Engineering,* **18**(3), 3, pp. 323–341.
[53] Babuska, I., Szabo, B. A., and Katz, I. N., 1981. "The p-version of the finite element method". *SIAM Journal on Numerical Analysis,* **18**(3), 6, pp. 515–545.
[54] Wolfram Research, Inc., 2020. Mathematica, Version 10.3. Champaign, IL.

A Formal Order of Accuracy: Spatial order

To establish the spatial formal order of accuracy of an FE solution algorithm, we provide a heuristic derivation [28, 48] and point the reader to more mathematically rigorous analyses with the same result [49, 50, 51, 52]. In this work, the convergence of the computed solution to the analytical solution is analyzed as the size of the FE approaches zero, e.g., h-convergence. No effort is made to quantify p-convergence, in which convergence is analyzed as the order of the basis functions is increased [53]. For derivation of the formal order of accuracy for temporal analysis, see [9].

For the problems in this work, there are no singularities in mesh, properties, or external sources. All analytical solutions are continuous, smooth, and infinitely differentiable. The mesh has constant spacing and is uniformly refined. Under these conditions, the analysis of the discretization error is relatively simple. Here, we will analyze the behavior of the error in the temperature T at some specified point in the domain x^*, and use the results to make generalizations about the entire domain. First, note that the exact solution to a specific problem can be represented by a Taylor series about some point $\hat{x}$ in the FE that contains x^*:

$$T(x) = \sum_{n=0}^{\infty} \frac{1}{n!} \left. \frac{d^n T}{dx^n} \right|_{\hat{x}} (x-\hat{x})^n. \tag{24}$$

This expansion assumes that $T(x)$ is infinitely differentiable, which is true for all solutions in this work. Here, we have used a Taylor series approximation, which corresponds to a polynomial basis function of degree p. Note that this procedure is equally applicable to other basis functions. The approximate solution calculated by the simulation tool $\tilde{T}$ using the chosen basis function of degree p is

$$\tilde{T}(x) = \sum_{n=0}^{p} a_n (x-\hat{x})^n. \tag{25}$$

The Taylor series coefficients have been collapsed into the arbitrary constant a_n. We define the length of an element as h and note that $|x-\hat{x}| \leq h$ because $\hat{x}$ is a point inside the element. As the mesh is uniformly refined, $h \to 0$, the approximate solution $\tilde{T}$ approaches arbitrarily close to the terms of Eqn. 24 which are degree p or lower. In addition, the domain point x^* approaches the FE point $\hat{x}$ as the mesh is refined. Therefore, the remaining terms of $p+1$ and greater will form the error at point x^*.

$$T(x^*) - \tilde{T}(x^*) \to \sum_{n=p+1}^{\infty} c_n (x-\hat{x})^n, \quad \text{as } h \to 0. \tag{26}$$

Note that c_n is a constant which includes the coefficient and derivative term from Eqn. 24. For a sufficiently small h, higher order terms become negligible and the $p+1$ term will dominate.

$$T(x^*) - \tilde{T}(x^*) = c_{p+1} h^{p+1} \tag{27}$$

Now we generalize the point error in Eqn. 27 using a norm over all space:

$$||T(x)|| = Ch^{p+1}, \tag{28}$$

where C is an arbitrary constant that is problem-dependent and $||\cdot||$ indicates a norm.

All of the above arguments can also be applied to the heat flux, which is related to ∇T. Since the flux involves the first derivative of temperature, its asymptotic rate is one order lower than that of the function; therefore, its formal order is the same as the degree of the chosen FE:

$$|\nabla T(x)| = Ch^{p}, \tag{29}$$

where C is an arbitrary constant that is problem-dependent. Here, $|\cdot|$ denotes a semi-norm, which behaves mathematically as a norm, except that it can be zero for non-zero inputs. Note that this norm is sometimes referred to as the H_1-norm of temperature. Eqn. 8 can also be used to estimate the observed order of accuracy $\hat{p}$ for the heat flux.

B Derivations of New Analytic Solutions

The derivation of the analytic solutions in this work generally follow similar processes. Therefore, we provide an outline of the derivation without many details for each of the new problems derived for this work. Each solution is confirmed through (1) substitution of the analytic solution into the original problem statement, (2) comparison of the analytic solution to a Mathematica [54] solution, and (3) comparison of the analytic solution to a FE solution. Given these confirmation steps, we have established high confidence that the derived analytic solutions are correct. The problem settings for each problem are described in section 4.

Problem I.4: The heat conduction equation in Cartesian coordinates for Problem I.4 must satisfy the boundary conditions: (1) $-kdT/dx\big|_{x=0} = q''$ and (2) $-kdT/dx\big|_{x=L} = h(T-T_f)$.

$$-\frac{d}{dx}\left(k\frac{dT}{dx}\right) = q''' \tag{30}$$

The characteristic solution for this problem is

$$T(x) = -\frac{q'''x^2}{2k} + C_1 x + C_2, \tag{31}$$

where C_1 and C_2 are constants to be determined. The first boundary condition yields $C_1 = -q''/k$. The second boundary condition in combination with the known C_1 yields

$$C_2 = T_f + \frac{q'''L^2}{2k} + \frac{q''L}{k} + \frac{q'''L+q''}{h}. \tag{32}$$

Inserting C_1 and C_2 into Eqn. 31, the temperature distribution becomes Eqn. 12.

Problem I.5: The heat conduction equation in Cartesian coordinates for Problem I.5 must satisfy the boundary conditions: (1) $-dT/dx|_{x=0} = 0$ and (2) $T(x = L) = T_L$.

$$-\frac{d}{dx}\left(k\frac{dT}{dx}\right) = q'''_o\left(1-\frac{\beta x}{L}\right) \tag{33}$$

Integrating Eqn. 33 over dx results in the following expression:

$$\frac{dT}{dx} = -\frac{q'''_o}{k}\left(x-\frac{\beta x^2}{2L}\right)+C_1, \tag{34}$$

where C_1 is a constant to be determined. The first boundary condition is satisfied with $C_1 = 0$. Similarly, Eqn. 34 is integrated over dx, which yields:

$$T(x) = -\frac{q'''_o}{k}\left(\frac{x^2}{2}-\frac{\beta x^3}{6L}\right)+C_2, \tag{35}$$

where C_2 is a constant to be determined. The second boundary condition is employed to obtain an expression for C_2:

$$C_2 = T_L + \frac{q'''_o L^2}{2k}\left(1-\frac{\beta}{3}\right). \tag{36}$$

Inserting C_2 into Eqn. 35, the temperature distribution becomes Eqn. 13.

Problem II.1: The heat conduction equation in cylindrical coordinates for Problem II.1 must satisfy the boundary conditions: (1) $T(r = r_i) = T_i$ and (2) $T(r = r_o) = T_o$.

$$-\frac{1}{r}\frac{d}{dr}\left(kr\frac{dT}{dr}\right) = q''' \tag{37}$$

Double integration over dr results in

$$T(r) = -\frac{q'''r^2}{4k} + C_1\ln(r) + C_2, \tag{38}$$

where C_1 and C_2 are constants to be determined. The boundary conditions are used to obtain expressions for C_1 and C_2:

$$C_1 = \frac{1}{\ln(r_i/r_o)}\left[T_i - T_o + \frac{q'''}{4k}\left(r_i^2 - r_o^2\right)\right], \tag{39}$$

and

$$C_2 = T_o + \frac{q''' r_o^2}{4k} - \frac{\ln(r)}{\ln(r_i/r_o)} \left[T_i - T_o + \frac{q'''}{4k} \left(r_i^2 - r_o^2 \right) \right]. \tag{40}$$

Inserting these expressions into Eqn. 38, the temperature distribution becomes Eqn. 14.

Problem II.5: The heat conduction equation in cylindrical coordinates for Problem II.5 must satisfy the boundary conditions: (1) $T(r \to 0) \Rightarrow$finite (i.e., the finiteness requirement) and (2) $T(r = r_o) = T_o$.

$$-\frac{1}{r}\frac{d}{dr}\left(kr\frac{dT}{dr} \right) = q_o''' \left(1 - \beta \frac{r}{r_o} \right) \tag{41}$$

Double integration over dr results in the following expression:

$$T(r) = -\frac{q_o'''}{4k} \left(r^2 - \frac{4\beta}{9} \frac{r^3}{r_o} \right) + C_1 \ln(r) + C_2, \tag{42}$$

where C_1 and C_2 are constants to be determined. The first boundary condition is satisfied with $C_1 = 0$. The second boundary condition is employed to obtain an expression for C_2, yielding

$$C_2 = T_o + \frac{q_o''' r_o^2}{4k} \left(1 - \frac{4\beta}{9} \right). \tag{43}$$

Inserting C_2 into Eqn. 42, the temperature distribution becomes Eqn. 18.

Problem III.3: The heat conduction equation in spherical coordinates for Problem III.3 must satisfy the boundary conditions: (1) $T(r = r_i) = T_o$ and (2) $T(r = r_o) = T_o$.

$$-\frac{1}{r^2}\frac{d}{dr}\left(kr^2\frac{dT}{dr} \right) = q''' \tag{44}$$

The characteristic solution for this problem is

$$T(r) = -\frac{q''' r^2}{6k} + \frac{C_1}{r} + C_2, \tag{45}$$

where C_1 and C_2 are constants to be determined.

The integration constants are evaluated by application of a *Kirchhoff transformation*. We introduce an auxiliary variable u with a constant k_c. Thus, $k_c \frac{du}{dr} = k_T \frac{dT}{dr}$ with satisfying the boundary conditions of $u = T_1$ at $r = r_1$ and $u = T_2$ at $r = r_2$. The particular solution satisfying these for the simplest case of $T_1 = T_2 = 0$ in terms of u is

$$u = \frac{q'''}{6k} \left(r_o^2 - r^2 \right) - \frac{q'''}{6k} \left(r_o^2 - r_i^2 \right) \frac{\left(\frac{1}{r} - \frac{1}{r_o} \right)}{\left(\frac{1}{r_i} - \frac{1}{r_o} \right)}. \tag{46}$$

The original dependent variable is $T = T(u)$. For the case of linearly increasing conductivity,

$$k_c \int_{u=T_1}^{u} du = \int_{T_1}^{T} k_T dT = k_0 \int_{T_1}^{T} (1+\beta T) dT \tag{47}$$

whereby

$$\frac{\beta}{2} T^2 + T - \left[T_1 + \frac{\beta}{2} T_1^2 - \frac{k_c}{k_0} (T_1 - u) \right] = 0, \tag{48}$$

which is a quadratic equation.

$$k_c \int_{u=T_1}^{u=T_2} du = k_0 \int_{T_1}^{T_2} (1+\beta T) dT \quad \rightarrow \quad k_c = k_0 \left[1 + \frac{\beta}{2} (T_1 + T_2) \right] \tag{49}$$

such that $k_c = k_0$ for the simplest case of $T_1 = T_2 = 0$.

The semidefinite integration of du gives $T = T(u)$ for $T_1 = 0$ in Eqn. 47 as $\frac{\beta}{2} T^2 + AT - k_c u = 0$. Solving this quadratic equation yields the following expression for T [39, p.194]:

$$T = \frac{1}{\beta} \left(\sqrt{1 + 2\beta\Omega} - 1 \right), \tag{50}$$

in which

$$\Omega = \frac{q'''}{6k_o} \left[(r_o^2 - r^2) - \left(r_o^2 - r_i^2 \right) \frac{\left(\frac{1}{r} - \frac{1}{r_o} \right)}{\left(\frac{1}{r_i} - \frac{1}{r_o} \right)} \right]. \tag{51}$$

Substituting Eqn. 51 into Eqn. 50, the temperature distribution becomes Eqn. 21.

Problem III.4: The heat equation in spherical coordinates for Problem III.4 must satisfy the boundary conditions: (1) $-kdT/dr\big|_{r=r_i} = q_i''$ and (2) $-kdT/dr\big|_{r=r_o} = h(T - T_f)$.

$$-\frac{1}{r^2} \frac{d}{dr} \left(kr^2 \frac{dT}{dr} \right) = q''' \tag{52}$$

The characteristic solution for this problem is

$$T(r) = -\frac{q''' r^2}{6k} + \frac{C_1}{r} + C_2, \tag{53}$$

where C_1 and C_2 are constants to be determined. The first and second boundary conditions yield expressions for C_1 and C_2, respectively:

$$C_1 = \frac{q_i'' r_i^2}{k} - \frac{q''' r_i^3}{3k}, \tag{54}$$

and

$$C_2 = T_f + \frac{q'''}{6k}\left[r_o^2 + \frac{2k}{hr_o^2}\left(r_o^3 - r_i^3\right) + \frac{2r_i^3}{r_o}\right] + \frac{q_i'' r_i^2}{k}\left[\frac{k}{hr_o^2} - \frac{1}{r_o}\right]. \tag{55}$$

Substituting C_1 and C_2 into Eqn. 53, the temperature distribution becomes Eqn. 22.